Viscosity Dependence of Chain Segemental Motion and Side-Chain Internal Rotation of Poly(1-naphthylmethyl acrylate) in Dilute Solution. Carbon-13 Nuclear Magnetic Relaxation Study

Apostolos Spyros and Photis Dais*

Department of Chemistry, University of Crete, 71409 Iraklion, Crete, Greece

Frank Heatley*

Department of Chemistry, University of Manchester, Manchester M13 9PL, U.K.

Received May 14, 1994; Revised Manuscript Received July 15, 1994®

ABSTRACT: Chain segmental motion and side-chain internal rotation of poly(1-naphthylmethyl acrylate) in dilute solution have been studied by employing the ^{13}C nuclear magnetic relaxation technique. Correlation times and diffusion constants were determined through dynamic modeling of the various modes of reorientation occurring in this polymer as a function of temperature and solvent viscosity. Local segmental motion and naphthyl internal rotation appear to follow Kramers' theory, whereas the correlation time for the side-chain methylene internal motion scales as $\eta^{0.55}$, instead of the first power dependence predicted by Kramers' theory. The potential energy heights extracted from these measurements were found to be 11, 21, and 5.5 kJ mol^{-1} for segmental motion, naphthyl restricted internal rotation, and methylene restricted internal rotation, respectively. Furthermore, on the basis of our data some general conclusions were drawn regarding solvent effects on the expected photophysical behavior of poly(1-naphthylalkyl acrylate)s.

Introduction

The photophysical behavior of polymer systems containing pendant naphthalene groups has been investigated extensively in the past,[1,2] in an attempt to mimic energy transfer process in plant photosynthesis and understand the mechanisms of photodegradation and/or photostabilization of commercial polymers. In two recent reports,[3,4] we examined the microstructure and the dynamics of a series of poly(1-naphthylalkyl acrylate)s in 1,1,2,2-tetrachloroethane (TCE) solution by using ^{13}C NMR spectroscopy, in order to correlate molecular structure and dynamic properties of these polymers with their ability in forming excimers between the naphthalene chromophores. In this paper we focus our attention on the influence of solvent viscosity on local dynamics of the second member of this class of polymers, poly(1-naphthylmethyl acrylate) (PNMA), in dilute solution by employing the ^{13}C nuclear magnetic relaxation technique.

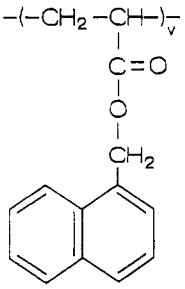

PNMA

The first goal of the present study is to examine the extent to which the various modes of reorientation of PNMA, e.g., chain segmental motion and naphthyl internal rotation about the CH_2–C(1) bond, are affected by solvent–polymer interaction. Photophysical results have shown[5] that excimer formation between the naphthyl groups in poly(1-naphthylalkyl acrylate)s is only slightly affected by changing the solvent.

The present work is also motivated by a desire to examine the validity of Kramers' theory[6] for this complex polymer system. There seems to be a general consensus in the literature that correlation times, describing local dynamics, increase with solvent viscosity, but the functional form of this relationship appears to depend on the experimental technique used to study polymer dynamics, the polymer structure, the nature of the solvent systems, and the range of viscosity covered by the solvents. Techniques such as NMR that sense very rapid local chain motions involving one to two monomer units may not follow the viscosity dependence as described by Kramers' equation. Such deviations have been reported in NMR studies on two systems.[7,8] On the other hand, optical techniques that probe motions over a slightly longer length scale (~5–10 monomer units) are more likely to follow Kramers' equation.[9] Moreover, strong solvent–polymer interactions or systems where hydrogen bonding occurs are expected to lead to a failure of Kramers' approach.[7]

Experimental Section

The synthesis of the monomer used to obtain the polymer PNMA and the polymerization procedure have been described in detail in an earlier publication.[3]

NMR Measurements. ^{13}C NMR relaxation measurements were conducted at ^{13}C Larmor frequencies of 125.7 and 75.4 MHz on Varian Unity 500 and XL-300 spectrometers under broadband proton decoupling. The sample temperature was controlled to within ±1 °C by means by precalibrated thermocouples in the probe inserts.

The spin–lattice relaxation times (T_1) were measured by the standard IRFT method with a repetition time longer than $5T_1$. A total of 512 acquisitions was accumulated, for a set of 8–10 "arrayed" τ values. Values of T_1 were determined by a three-parameter nonlinear procedure with a rms error of ±10% or better. NOE experiments were carried out by inverse gated decoupling, at least two experiments being performed for each temperature value. Delays of at least 10 times the longest T_1

® Abstract published in *Advance ACS Abstracts*, September 1, 1994.

0024-9297/94/2227-6207$04.50/0

were used between 90° pulses. NOE values are estimated to be accurate within ±15%. Measurements of ^{13}C spin–spin relaxation times (T_2) were performed by using the Carr–Purcell–Meiboom–Gill[10] (CPMG) pulse sequence with complete broad-band decoupling of protons. However, to avoid an irreversible diminution in the measured T_2 values as compared to the true values,[11] decoupling was switched off during echo formation but reestablished during acquisition and over a long delay time ($\sim 5T_1$) before the repetition of the pulse sequence. The duration of the 180° pulse train covered a range of about 0.01–3 times the longest T_2 value. The accuracy of the measured T_2 values is estimated to be ±15–20%.

Samples of PNMA in pentachloroethane (PCE) and deuteriochloroform (0.1 g cm^{-3}) were degassed by several freeze–pump–thaw cycles and sealed in 5 mm NMR tubes. Nevertheless, measurements with undegassed samples did not show any measurable change in the ^{13}C relaxation parameters relative to those of the degassed samples.

Viscosity measurements were performed using an Ubbelohde type dilution viscometer at 30 °C. For PNMA solutions in PCE and $CDCl_3$ solvents the intrinsic viscosities ([η]) and Huggins' constants (k') in eq 1 were found to be 0.222 and 2.084 and 0.221 and 1.124, respectively.

$$\eta_{sp}/C = [\eta] + k'[\eta]^2 C \qquad (1)$$

Numerical Calculations. The relaxation data were analyzed by using the MOLDYN program,[12] modified to include the spectral density functions of the various models used in the present study. Details of the program and the fitting procedure by employing various models for the backbone and side-chain motions have been given elsewhere.[12-14]

Results and Discussion

Analysis of the NMR Relaxation Data. The NT_1 values measured at 75.4 and 125.7 MHz for the backbone methine and methylene carbons of PNMA in PCE and chloroform are plotted as a function of temperature in Figures 1 and 2, respectively. Figures 3 and 4 show similar plots for the NOE values of the backbone carbons. Also, the NT_2 values for the same carbons measured at 125.7 MHz in both solvents are shown in Figures 1 and 2. Inspection of Figures 1–4 reveals a number of motional characteristics that are commonly observed in the ^{13}C relaxation data of most polymeric materials: (1) as the temperature increases, the NT_1 values decrease monotonically, in both fields, reaching a minimum which is followed by an increase in NT_1 with further increase in temperature; (2) the minimum is shifted to higher temperatures (shorter correlation times) as the magnetic field increases; (3) at a given temperature and solvent, NT_1 values increase with increasing magnetic field. The difference in NT_1 values between the two magnetic fields becomes more pronounced as the temperature decreases (slow motion regime); (4) the NT_2 values decrease continually with decreasing temperature, and they are always much smaller than the NT_1 values, especially at low temperatures; (5) the NOE values decrease with increasing magnetic field, although they tend to converge as temperature decreases, reaching the slow motion regime; (6) both NT_1 and NOE transitions are much broader than for small molecules; (7) at high temperatures, where motion becomes faster, NOE values are less than the theoretical maximum.

An interesting feature of the data is that in both solvents the ratio of T_1 values of the CH and CH_2 groups, $T_1(CH)/T_1(CH_2)$, as determined in both magnetic fields, is fairly constant at 1.82 ± 0.05 in $CDCl_3$ and 1.83 ± 0.04 in PCE throughout the temperature range studied. This value is different from the value of 2, which is expected from the number of directly bonded proton and suggests different

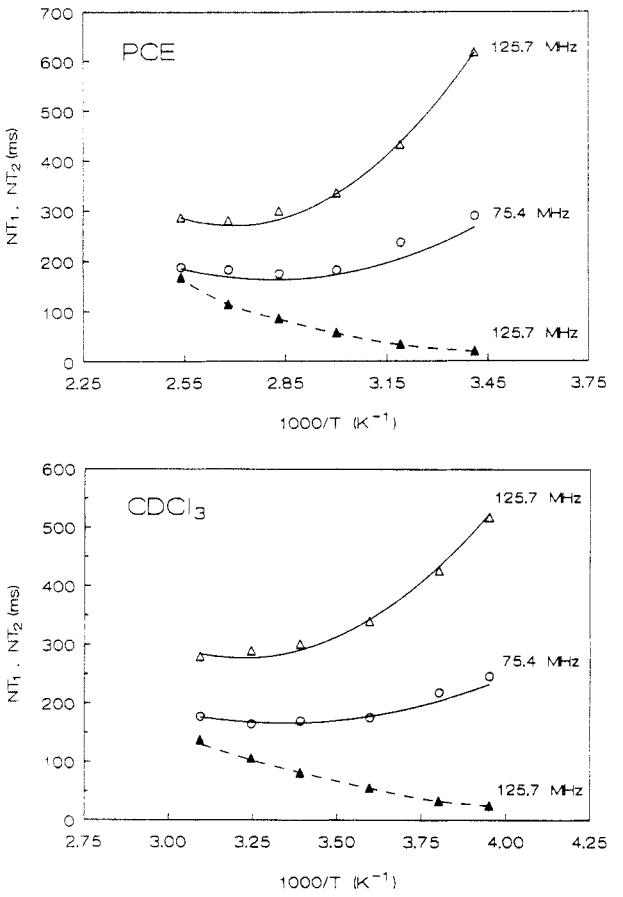

Figure 1. Experimental spin–lattice relaxation times (NT_1, open symbols) and spin–spin relaxation times (NT_2, filled symbols) for the backbone methine carbon of PNMA in PCE and $CDCl_3$ solutions as a function of temperature and magnetic field. Solid and dashed lines represent the best fit values calculated by using the DLM model.

local motions for the C–H internuclear vectors associated with the CH and CH_2 groups.

Figure 5 illustrates the temperature behavior of the NT_1, and NT_2 values of the side-chain methylene carbon in the two solvents. As expected[4,15] for the faster side-chain motions relative to the backbone motion, i.e., motions within the "fast motion regime", the NT_1 values increase with increasing temperature, although they pass through a minimum NT_1 value. This minimum occurs at a lower temperature in chloroform than in PCE solution as observed in the NT_1 vs $1/T$ curves of the backbone motions (compare Figure 5 with Figures 1 and 2). The temperature dependence of the NOE values of the side-chain methylene carbon at two magnetic fields in both solvents is illustrated in Figure 6. The NOE values follow the same temperature and magnetic field dependence as the NOE values of the backbone carbon (Figures 3 and 4), although the former values are greater than the latter at each temperature, reflecting the faster motion of the side chain.

Figures 7 and 8 illustrate the variation of the average relaxation parameters NT_1, NT_2, and NOE of the C-2, C-3, C-6, and C-7 carbons of the naphthyl moiety as a function of temperature and magnetic field in PCE and chloroform solvents, respectively. The relaxation parameters of these carbons are similar to each other and systematically greater than those of the C-4, C-5, and C-8 carbons in both solvents, especially at the high field. This is consistent with the fact[4,15] that the C–H vectors of the former group of carbons are oriented at an angle of ca. 60° with respect to the naphthyl internal rotation axis, and

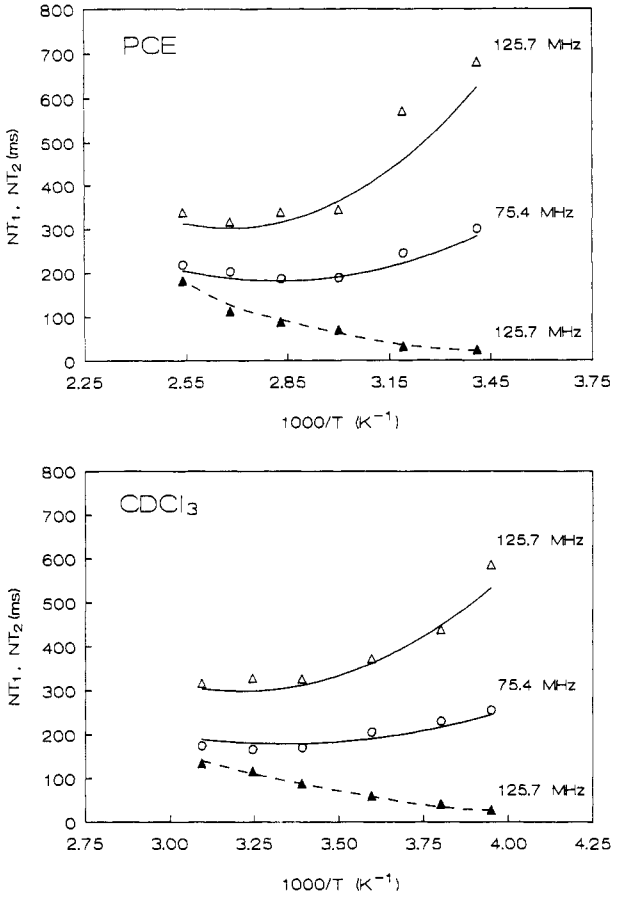

Figure 2. Experimental spin–lattice relaxation times (NT_1, open symbols) and spin–spin relaxation times (NT_2, filled symbols) for the backbone methylene carbon of PNMA in PCE and $CDCl_3$ solutions as a function of temperature and magnetic field. Solid and dashed lines represent the best fit values calculated by using the DLM model.

therefore their relaxation parameters are influenced by the motion about this axis, whereas the C–H bond vectors of the latter group of carbons are parallel to this axis, and hence their relaxation parameters are not affected by the rate of naphthyl internal rotation.

More information on the detailed nature of the intramolecular processes occurring in PNMA polymer can be obtained from a quantitative interpretation of the NMR relaxation parameters through dynamic modeling. In modeling the dynamics of PNMA, three types of motion are considered: (1) the overall rotatory diffusion of the polymer chain as a whole, (2) backbone segmental motion, and (3) side-chain motion. Each of these motions is considered as an independent source of motional modulation of the ^{13}C–^{1}H dipole–dipole interactions for the protonated carbons of PNMA.

In polymers, the dominant relaxation process is the ^{13}C–^{1}H dipolar interactions.[16] Also, for these systems, only interactions with directly bonded protons need be considered.[4,7,15] Under conditions of complete proton decoupling, the ^{13}C relaxation parameters, T_1, T_2, and NOE, can be written in terms of the spectral density function, $J(\omega_i)$[7,13,17]

$$\frac{1}{T_1^{DD}} = \frac{\Omega}{10}[J(\omega_H-\omega_C) + 3J(\omega_C) + 6J(\omega_H+\omega_C)] \quad (2)$$

$$\frac{1}{T_2^{DD}} = \frac{1}{2T_1^{DD}} + \frac{\Omega}{20}[4J(0) + 6J(\omega_H)] \quad (3)$$

$$\mathrm{NOE} = 1 + \frac{\gamma_H}{\gamma_C}\left[\frac{6J(\omega_H+\omega_C) - J(\omega_H-\omega_C)}{J(\omega_H-\omega_C) + 3J(\omega_C) + 6J(\omega_H+\omega_C)}\right] \quad (4)$$

and

$$\Omega = N\left(\frac{\mu_0\gamma_H\gamma_C h}{8\pi^2 r_{CH}^{\ 3}}\right)^2$$

where γ_H and γ_C are the gyromagnetic ratios of the proton and carbon nuclei, respectively, ω_H and ω_C and their Larmor frequencies, μ_0 is the vacuum magnetic permeability, h is Planck's constant, N is the number of directly bonded protons, and r_{CH} is the C–H internuclear distance (taken to be 1.09 Å for the methine and methylene carbons, and 1.08 Å for the aromatic carbons). $J(\omega_i)$ is related to the normalized time-correlation function (TCF), $G(t)$, that embodies all the information about mechanisms and rates of the various motional processes.

$$J(\omega_i) = \frac{1}{2}\int_{-\infty}^{+\infty} G(t)e^{i\omega t}\,dt \quad (5)$$

The assumption of independent motions allows the total TCF to be expressed as a product of the TCFs associated with each motional process.

The mechanism of chemical shift anisotropy (CSA) is expected to contribute to the relaxation of the aromatic carbons of the naphthyl moiety at high magnetic fields. Equations 2–4 can be modified to include this contribution.[4,7,17]

$$\frac{1}{T_i^{obs}} = \frac{1}{T_i^{DD}} + \frac{1}{T_i^{CSA}} \qquad (i = 1, 2) \quad (6)$$

where T_1^{DD} and T_2^{DD} are the dipole–dipole contributions as in eqs 2 and 3 and T_1^{CSA} and T_2^{CSA} are contributions from the chemical shift anisotropy mechanism. If the chemical shift tensor is axially symmetric, T_1^{CSA} and T_2^{CSA} are given by[4,7,17]

$$\frac{1}{T_1^{CSA}} = (2/15)\omega_C^{\ 2}\Delta\sigma^2 J(\omega_C) \quad (7)$$

$$\frac{1}{T_2^{CSA}} = (1/45)\omega_C^{\ 2}\Delta\sigma^2[4J(0) + 3J(\omega_C)] \quad (8)$$

where

$$\Delta\sigma = \sigma_{33} - \frac{1}{2}(\sigma_{11} + \sigma_{22})$$

The NOE is given by eq 9 combining eqs 2, 4, 6, and 7; i.e

$$\mathrm{NOE} = 1 + \left(\frac{\gamma_H}{\gamma_C}\right)\{[(\Omega/10)[6J(\omega_H+\omega_C) - J(\omega_H-\omega_C)]]/ [(\Omega/10)[J(\omega_H-\omega_C) + 3J(\omega_C) + 6J(\omega_H+\omega_C)] + (2/15)\omega_C^{\ 2}\Delta\sigma^2 J(\omega_C)]\} \quad (9)$$

The use of eqs 7–9 is an approximation, since the chemical shift tensor of the protonated carbons of the naphthyl group may not be axially symmetric as has been observed experimentally for naphthalene in the solid.[4,18] Nevertheless in the latter molecule, the low-field major components of the tensors are directed approximately along the C–H bonds,[18] indicating that one of the vectors whose motion leads to CSA relaxation is nearly parallel to the aromatic C–H bond. In the present calculations, we have ignored higher order effects and fitted our data to eqs 6–9 with an

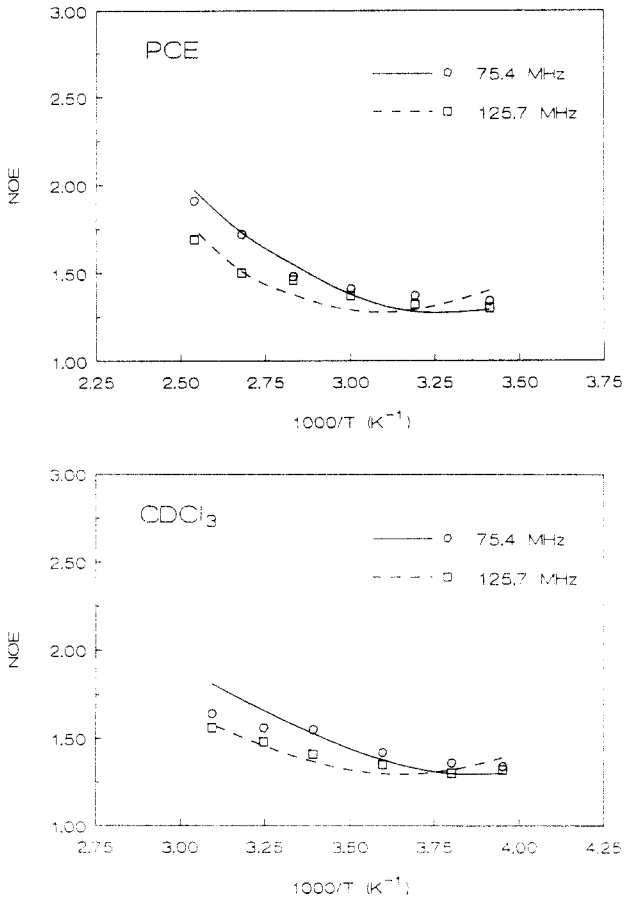

Figure 3. Experimental NOE values for the backbone methine carbon of PNMA in PCE and $CDCl_3$ solutions as a function of temperature and magnetic field. Solid and dashed lines represent the best fit values calculated by using the DLM model.

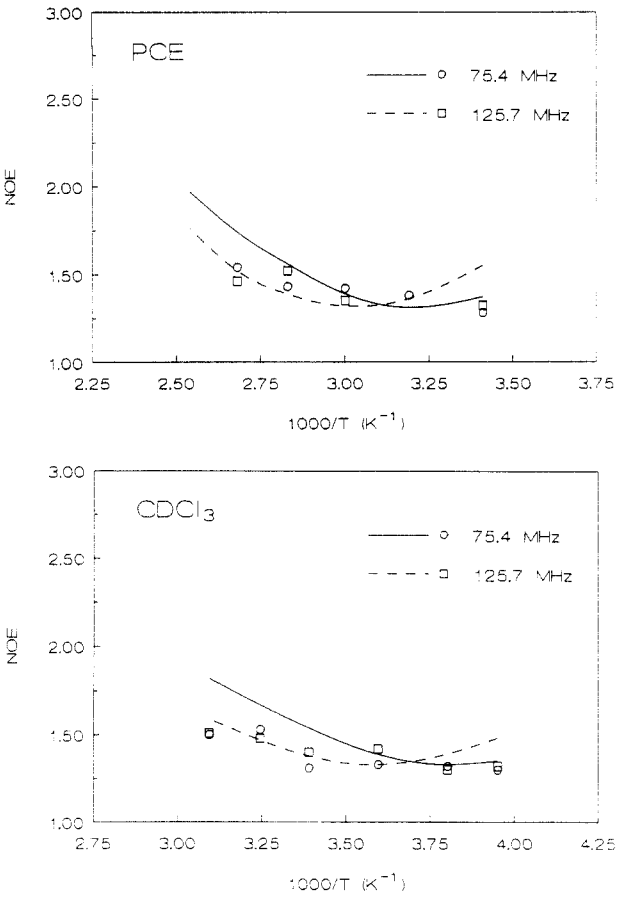

Figure 4. Experimental NOE values for the backbone methylene carbon of PNMA in PCE and $CDCl_3$ solutions as a function of temperature and magnetic field. Solid and dashed lines represent the best fit values calculated by using the DLM model.

average $\Delta\sigma$ = 167 ppm value obtained from the principal values of the ^{13}C shift tensor of the protonated carbons of naphthalene.[18]

For sufficiently high molecular weight polymers, the overall motion is much slower than the chain local motions and thus makes a negligible contribution to the relaxation of the backbone and side-chain carbons.[4,13,14,19] This conclusion is supported by the long correlation time, τ_R, estimated at infinite dilution as a function of the molecular weight, M, and the intrinsic viscosity, $[\eta]$, of the polymer solution in a given solvent of viscosity, η, through the hydrodynamic equation[20]

$$\tau_R = \frac{2M[\eta]\eta}{3RT} \tag{10}$$

which was found to be 1.15×10^{-6} s in chloroform and 4.6×10^{-6} s in PCE at 30 °C.

The next motions considered are the local motions and these are backbone segmental motion and side-chain internal rotations. Segmental motion of PNMA in dideuterio-1,1,2,2-tetrachloroethane solution (TCE-d_2) has been described[4] successfully by using a model developed by Dejean, Laupretre, and Monnerie[21] (DLM). This model describes the backbone reorientation in terms of two independent kinds of motion: (1) a diffusional process along the chain, which occurs via conformational transitions described[22] by two correlation times τ_0 and τ_1 for isolated, single-bond conformatioanl transitions and for cooperative transitions, respectively, and (2) bond librations, i.e., wobbling in a cone motion of the backbone internuclear C–H vectors as described by Howarth.[23] The librational motion is associated with a correlation time τ_2, whereas the extent of the libration about the rest position of the C–H bond (the axis of the cone) is determined by the cone half-angle θ. The TCF of the DLM model and its Fourier transform, the spectral density, are given in the references cited.[4,14,21] Composite spectral density functions for side-chain motions superimposed on the polymer backbone motion have been developed recently[24] and applied[4] successfully to describe the dynamics of the side-chain of PMMA and other related polymers in TCE-d_2 solutions. Backbone conformational transitions are described by τ_0 and τ_1 correlation times, where the frequency-dependent relaxation data of the side-chain methylene and naphthyl carbons are better reproduced by considering multiple restricted rotations about the side-chain O–CH_2 and CH_2–C(1) bonds. The independent internal rotation about each bond is assumed to be diffusion within a square-well potential[25] and is expressed in terms of two phenomenological parameters, D_i and φ_i, which give the rate of diffusion and the width of the square well (i.e., the angular amplitude of the restricted rotation), respectively. The explicit form of the composite spectral density is given elsewhere.[4,24]

The simulation parameters of the models that reproduce the experimental data of PNMA in the two solvents and at the two fields are listed in Tables 1–3. Also, these tables summarize the simulation parameters of the models for PNMA in TCE-d_2, obtained from a previous study,[4] for comparison. The best fit of NT_1, NT_2, and NOE data is plotted in Figures 1–8 for all protonated carbons of PNMA. The agreement between experimental and theoretical values is very good throughout the entire temperature

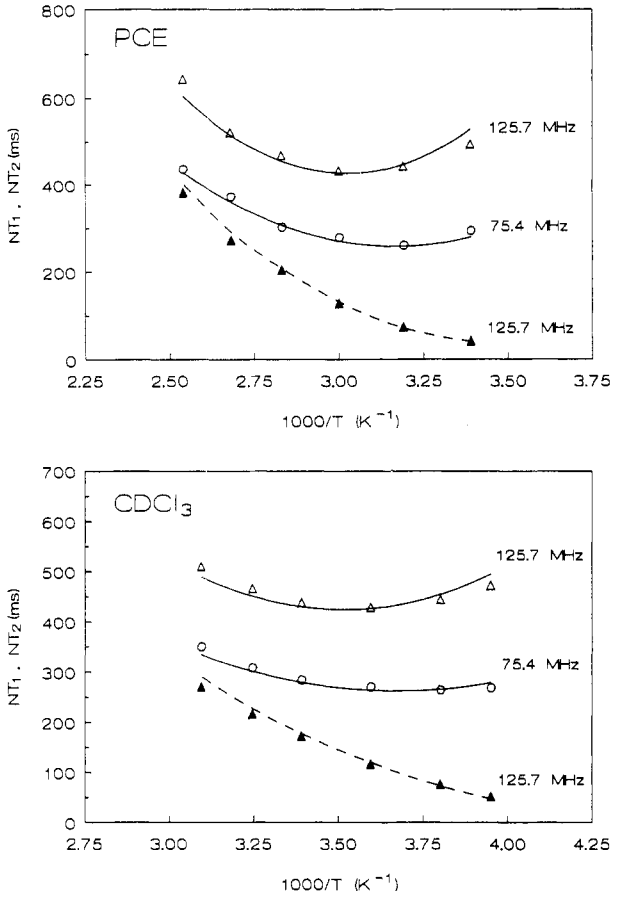

Figure 5. Experimental spin–lattice relaxation times (NT_1, open symbols) and spin–spin relaxation times (NT_2, filled symbols) for the side-chain methylene carbon of PNMA in PCE and $CDCl_3$ solutions as a function of temperature and magnetic field. Solid and dashed lines represent the best fit values calculated by using the composite spectral density of refs 4 and 24 (see text).

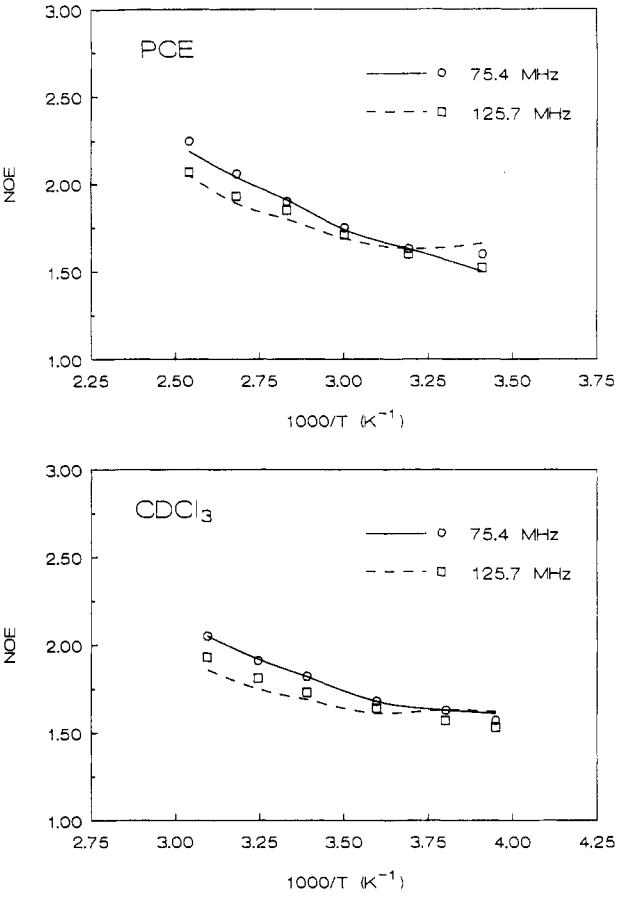

Figure 6. Experimental NOE values for the side-chain methylene carbon of PNMA in PCE and $CDCl_3$ solutions as a function of temperature and magnetic field. Solid and dashed lines represent the best fit values calculated by using the composite spectral density of refs 4 and 24 (see text).

studied and reflects the ability of the dynamic models adopted to describe the backbone and side-chain motions of PNMA in the two solvents.

The best fit half-angles of the librational motion of the C–H vectors for the methine carbon, θ_{CH}, are smaller than the corresponding half-angles, θ_{CH_2}, calculated for the backbone methylene carbon (Table 1). This observation explains the fact that $T_1(CH)/T_1(CH_2) < 2$ and supports the conclusion that θ is related to the steric hindrance at the considered site; the larger the steric hindrance, the smaller is θ.

It is of interest to note that both θ_{CH} and θ_{CH_2} values obtained for PNMA are independent of solvent viscosity. These values are nearly the same in the three solvents (Table 1). This observation is consistent with the fact that librational motion is a much faster motion than backbone conformational transitions, and hence it is only very weakly dependent on solvent viscosity. Solvent molecules move only slightly on the librational time scale, imposing no appreciable friction to the librational motion of the backbone C–H vectors. Recent experimental findings[26] lead to the same conclusion.

The τ_1 values derived from fitting the experimental relaxation data of PNMA in the three solvents with the DLM model are compiled in Table 1. A plot of the logarithm of these values as a function of $1/T$ shows linear correlations in the temperature range studied, yielding activation energies (E_a) of 20, 23, and 25 kJ mol^{-1} in chloroform, TCE, and PCE solvents, respectively.

The calculated diffusion constants, D_1 and D_{Np}, and the angular amplitudes, φ_1 and φ_{Np}, of restricted internal rotations about the O–CH_2 and CH_2–C(1) bonds, respectively, summarized in Tables 2 and 3, indicate the following trends of the side-chain motion: (1) internal rotations are restricted in nature characterized by amplitudes $2\varphi_i$ ranging between 60 and 150° in a temperature range of 140 °C; (2) the rate of internal rotation about the O–CH_2 bond is faster by an order of magnitude than the rate of rotation about the CH_2–C(1) bond in a given solvent; (3) the rates of internal motions about the O–CH_2 and CH_2–C(1) bonds increase progressively with decreasing solvent viscosity on going from PCE to chloroform; (4) the amplitude of restricted rotations does not change appreciably in the three solvents; and (5) the activation energies associated with the methylene internal rotation are nearly the same in the three solvents and much smaller than those of the naphthyl internal rotation in the same solvents. These observations underline the size of the reorientating units in the side chain of PNMA. The bulkier naphthyl moiety is expected to sweep out a larger volume of the solvent molecules during rotation about the CH_2–C(1) bond, and hence it experiences a larger hydrodynamic friction than the much smaller methylene group. This results in a slower rate and a higher apparent activation energy for the naphthyl internal rotations.

Viscosity Effects on PNMA Dynamics. Rates of conformational transitions in viscous media can be treated by the approach introduced by Kramers,[6] who studied the effects of solvent frictional forces on the rates of chemical reactions by modeling the reactive motion as the passage of a solute particle over a potential barrier. In this theory, which is based on the ordinary Langevin equation, the solvent is treated as a random frictional force

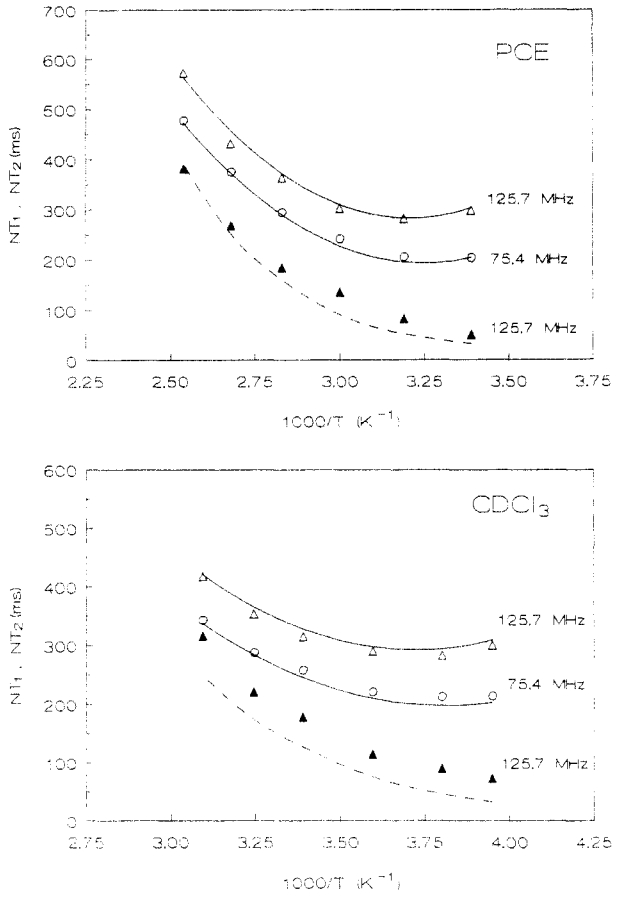

Figure 7. Experimental average spin–lattice relaxation times (NT_1, open symbols) and spin–spin relaxation times (NT_2, filled symbols) for the C-2, C-3, C-6 and C-7 carbons of the naphthyl group of PNMA in PCE and $CDCl_3$ solutions as a function of temperature and magnetic field. Solid and dashed lines represent the best fit values calculated by using the composite spectral density of refs 4 and 24 (see text).

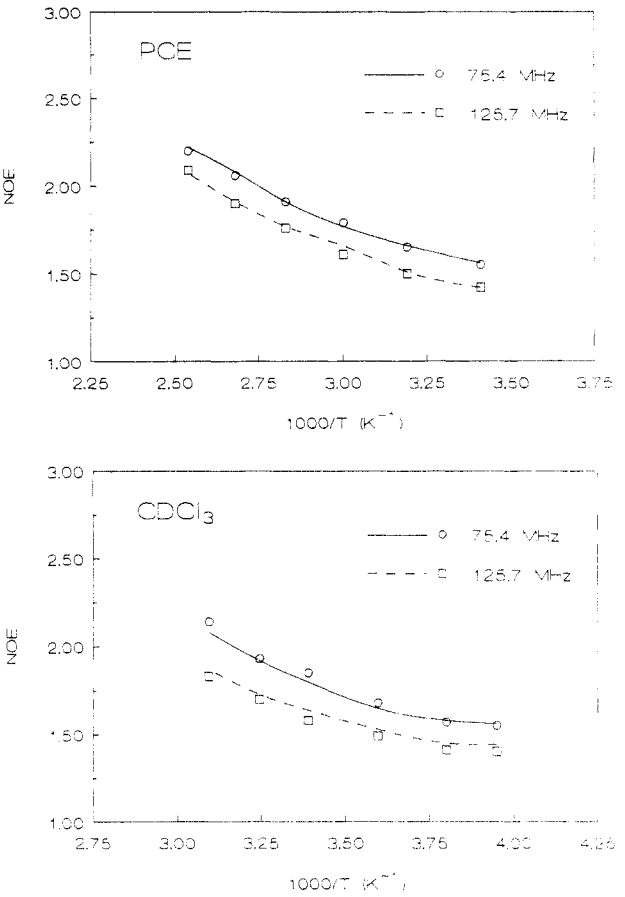

Figure 8. Experimental average NOE values for the C-2, C-3, C-6 and C-7 carbons of the naphthyl group of PNMA in PCE and $CDCl_3$ solutions as a function of temperature and magnetic field. Solid and dashed lines represent the best fit values calculated by using the composite spectral density of refs 4 and 24 (see text).

opposing the passage across the barrier, and correlations in space and time of the solvent forces acting on the solute particle are neglected.

Kramers's theory with hydrodynamic friction has been tested extensively in the past decade in many photochemical isomerization reactions in solution in an attempt to rationalize the viscosity dependence of the observed rate constants.[27,28] Also, Helfand has applied this theory to the case of conformational transitions of polymers.[29] Making the assumption that the correlation time for conformational transitions is inversely proportional to the rate constant for isomerization, the temperature and viscosity dependence of the correlation time is predicted by Kramers' theory to be[7]

$$\tau = A\eta \exp(E^*/RT) \tag{11}$$

The prefactor A is a viscosity-independent constant, E^* is the barrier height defined for conformational transitions, and η is the solvent viscosity. Equation 11 predicts a linear dependence of log τ on log η at a given temperature with slope equal to one.

The temperature dependence of the viscosity is often described by an Arrhenius form

$$\eta = \eta_0 \exp(E_\eta/RT) \tag{12}$$

then, eq 11 becomes

$$\tau = A' \exp[(E^* + E_\eta)/RT] \tag{13}$$

where A' is a constant. The sum of the barrier height for conformational transitions, E^*, and the activation energy for viscous flow, E_η, equals the experimental activation energy, E_a, obtained from a plot of ln τ vs $1/T$, i.e.

$$E_a = E^* + E_\eta \tag{14}$$

Any deviation from linearity in the plot of log τ vs log η, which may be observed at high viscosities, indicates that the Kramers' expressions 11 and 14 are insufficient to describe the experimental relaxation rates. The failure of Kramers' theory has been attributed[27,28,30] to the breakdown of its major hypothesis that solvent–polymer collisions are uncorrelated in space and time at the high-friction limit. When the motion near the top of the barrier takes place on a very short time scale (picoseconds or subpicoseconds), collisions may be significantly correlated, and the time scales for polymer and solvent motion are not cleanly separated. As a result of the curvature observed in the log τ vs log η plot, the experimental correlation times at high viscosities lay consistently lower than those predicted by Kramers' theory. Ediger and co-workers[7] suggested the following empirical equation to describe viscosity effects on local segmental dynamics of polyisoprene in dilute solutions.

$$\tau = A'\eta^\alpha \exp(E^*/RT) \tag{15}$$

This equation has been used by Fleming and co-workers[27] to describe the power law relationship observed between the isomerization rate constant and viscosity. The exponent α takes values in the range $1 > \alpha > 0.1$. For α =

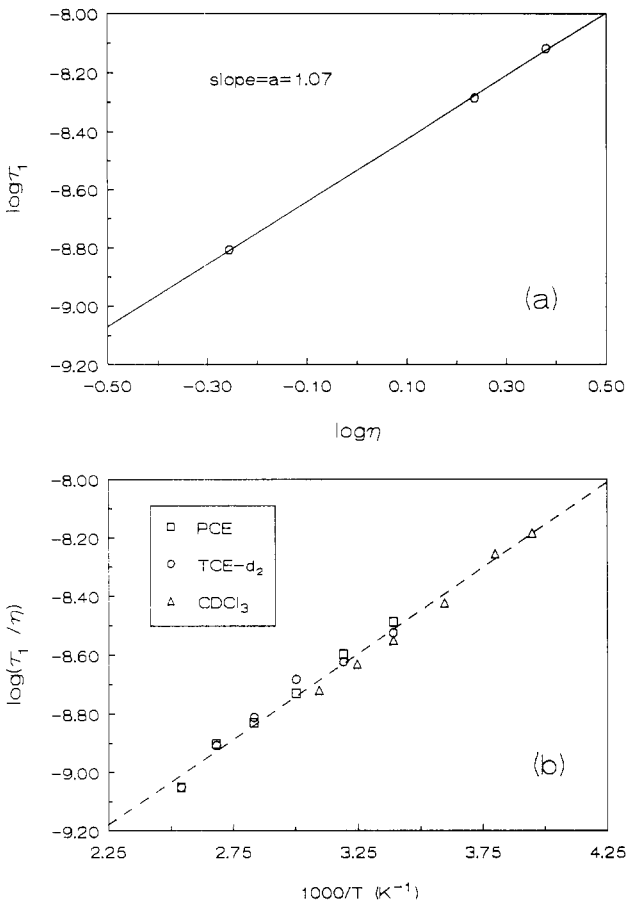

Figure 9. (a) Viscosity dependence of the correlation time τ_1 for the chain segmental motion of PNMA at 20 °C. (b) Temperature dependence of the reduced correlation time (τ_1/η) for the chain segmental motion of PNMA. All data points in Table 1 are included.

Table 1. Simulation Parameters of the DLM Model Used To Describe the Backbone Segmental Motion of PNMA in PCE, TCE-d_2, and $CDCl_3$

	τ_1 (ns)		
T (°C)	PCE	TCE-d_2[a]	$CDCl_3$
−20			6.00
−10			4.44
5			2.51
20	7.57	5.14	1.56
35			1.14
40	4.42	3.06	
50			0.81
60	2.39	2.02	
80	1.45	1.18	
100	0.96	0.77	
120	0.55	0.46	
τ_0/τ_1	7	5	7
τ_1/τ_2	100	50	80
θ_{CH}°	18.2	18.9	19.3
θ_{CH_2}°	23.6		23.1
E_α (kJ mol^{-1})	25	23	20
τ_∞ (10^{-12} s)	0.3	0.5	0.5
corr coeff	0.998	0.996	0.998

[a] Data from ref 4.

1 eqs 11 and 15 become identical. Also, eq 14 in the high-friction limit becomes

$$E_a = E^* + \alpha E_\eta \tag{16}$$

Figure 9a shows a plot of log τ_1 (τ_1 values are taken from Table 1) vs log η at 20 °C. The slope of this linear plot

Table 2. Simulation Parameters[a] of the Restricted Multiple Internal Rotations Model Used To Describe the Side-Chain O–CH_2 Motion of PNMA in PCE, TCE-d_2, and $CDCl_3$

	PCE		TCE-d_2[b]		$CDCl_3$	
T (°C)	D_1	φ_1°	D_1	φ_1°	D_1	φ_1°
−20					5.53	45
−10					6.56	49
5					8.47	51
20	4.24	47	5.66	53	9.85	55
35					12.57	57
40	6.09	49	7.28	55		
50					15.37	60
60	7.55	54	9.78	52		
80	9.27	61	12.20	62		
100	13.41	65	16.22	75		
120	16.87	74	21.60	75		
E_α (kJ mol^{-1})	13		13		10	
D_∞ (10^{12} s)	0.84		0.98		0.55	
corr coeff	0.993		0.995		0.996	

[a] D_1's × 10^9 s^{-1}. [b] Data from ref 4.

Table 3. Simulation Parameters[a] of the Restricted Multiple Internal Rotations Model Used To Describe the Side-Chain Naphthyl Motion of PNMA in PCE, TCE-d_2, and $CDCl_3$

	PCE		TCE-d_2[b]		$CDCl_3$	
T (°C)	D_{Np}	φ_{Np}°	D_{Np}	φ_{Np}°	D_{Np}	φ_{Np}°
−20					0.10	34
−10					0.11	32
5					0.53	28
20	0.14	46	0.19	43	1.45	37
35					2.10	42
40	0.22	41	0.48	38		
50					2.95	50
60	0.81	37	1.27	56		
80	2.17	45	2.33	62		
100	3.18	53	3.25	69		
120	4.86	58	5.52	70		
E_α (kJ mol^{-1})	37		32		33	
D_∞ (10^{14} s)	4.2		1.1		9.2	
corr coeff	0.986		0.994		0.990	

[a] D_{Np}'s × 10^9 s^{-1}. [b] Data from ref 4.

is very close to unity (α = 1.07), indicating that Kramers' theory is correct for the present polymer system in the range of viscosities studied. Figure 9b shows a plot of log (τ_1/η) vs $1/T$. The fact that a universal curve is obtained in all solvents supports the validity of Kramers' theory in describing the present experimental data without invoking frequency-dependent friction.[7,27,28,30] This implies that the observed activation energy is equal to the sum of the internal barrier and the viscosity activation energy (eq 14) and that the barrier height, E^*, is independent of viscosity. The value obtained from the best fit slope through the points of the plot in Figure 9b is 11.3 kJ mol^{-1}. This value is favorably compared with the barrier (12–14 kJ mol^{-1}) separating the trans and gauche states, indicating that the nature of the conformational transitions occurring in the PNMA chain can be described by the type 2* motion according to Helfand's terminology.[29] Type 2* motion is a cooperative conformational transition associated with an activation energy slightly higher than one barrier crossing.[29] During this transition the polymer tails undergo translation.[29]

Additional proof of the validity of Kramers' theory in describing segmental motion of PNMA is offered by the principle of frequency–temperature superposition[31] illustrated in Figure 10. This figure shows a plot of log-[ω_C/NT_1] versus log[$\omega_C\tau_1(T)$] that successfully superimposes a large number of NT_1 data for the methine carbon of PNMA in three solvents and various magnetic fields over

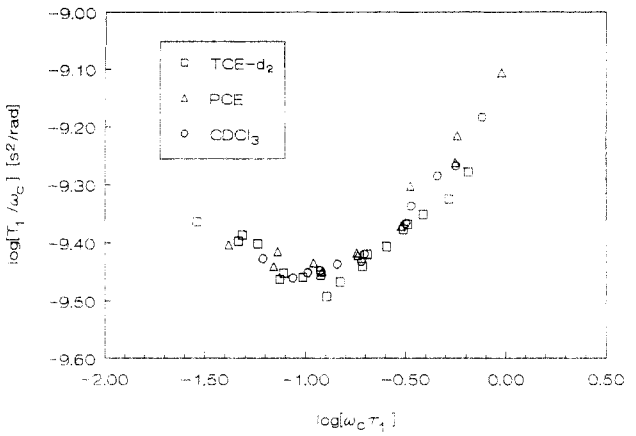

Figure 10. Frequency–temperature superposition of ^{13}C NMR NT_1 values for the backbone methine carbon of PNMA in PCE, TCE, and $CDCl_3$ solutions. τ_1 values are the correlation times obtained from the analysis of the relaxation data by using the DLM model (Table 1). The symbols correspond to different solvents.

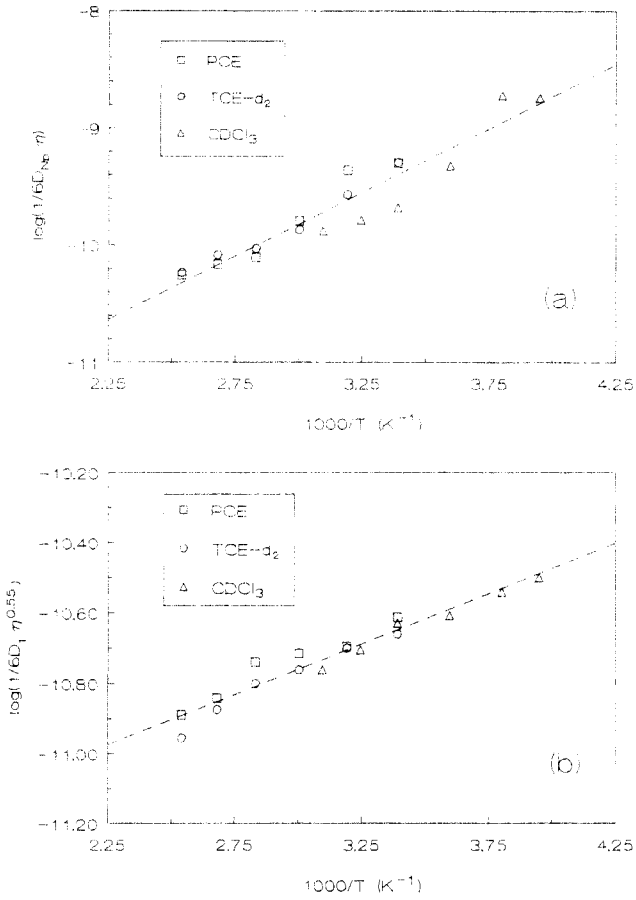

Figure 11. Temperature dependence of the reduced correlation times (a) ($\tau_{np}/\eta = 1/6D_{Np}\eta$) for naphthyl internal rotation and (b) ($\tau/\eta^{0.55} = 1/6D_1\eta^{0.55}$) for the side-chain methylene internal rotation of PNMA. All data points in Tables 2 and 3 are included.

the entire temperature range studied. τ_1 values are taken from Table 1. An analogous plot to that in Figure 9b for the correlation time τ_{np} ($=1/6D_{np}$) of naphthyl internal rotation is shown in Figure 11a. The fact that a universal curve is obtained when τ_{Np} is scaled by η indicates that the data indeed follow eq 11, reflecting Kramers' theory. The best fit slope of the straight line ($r = 0.96$) of Figure 11a yields an activation energy E^*_{Np} of 21 kJ mol^{-1}. This barrier of the naphthyl internal rotation about the CH_2–C(1) bond is within the range of 20–25 kJ mol^{-1} obtained in several photochemical isomerization reactions in solution.[27,28,32]

However, Kramers' theory appears to fail for the internal motion of the side-chain methylene group. The data in Figure 11b, i.e., correlation times for CH_2 in a format suggested by eq 15, conform with a universal curve when the correlation time is scaled by $\eta^{0.55}$. The best fit slope obtained through the points yields $E^* = 5.5$ kJ mol^{-1} for the internal motion of the side-chain CH_2 group. This value is consistent with the theoretical value of ~5 kJ mol^{-1} calculated for the barrier of the O–CH_2 bond rotation of poly(alkyl methacrylate)s and poly(methyl acrylate).[33,34]

One could be tempted to explain this result on the basis of the small size of the CH_2 moiety and the theory[30] that allows frequency-dependent solvent friction. Indeed, the exponent α depends on the moment of inertia, the size of the isomerizing unit, and the curvature of the potential energy surface at the top of the barrier.[7,28] Smaller size of the rotating unit, a smaller moment of inertia, and a high barrier all lead to an exponent α smaller than unity. Nevertheless, the present estimated barried E^* (=5.5 kJ mol^{-1}) for the methylene restricted internal rotation is only twice as large than that corresponding to kT (2.5 kJ mol^{-1} at $T = 298$ K). In this case, the breakdown of Kramers' theory cannot be attributed to details of solvent–solute coupling but rather to the fact that inertial effects may predominate on the internal rotation of the side-chain methylene carbon.[35]

Another solvent parameter that it is known to play a small role in determining the time scale and the activation energy for local conformational transitions is the solvent thermodynamic power. Optical[36,37] and NMR[14] studies have generally found that, after considering the solvent viscosity, dynamics in solvents of low thermodynamic quality (poor solvents) are slower by a factor of <2 than dynamics in solvents of high thermodynamic power (good solvents). Also, the activation energy, E^*, for conformational transitions is higher for poor solvents than for good solvents. This effect is considered to be steric in nature, and it is attributed to the higher local segment concentration in poor solvents.[36,37] The presence of nearby segments may interfere with a conformational transition that would otherwise be possible. The present study, however, shows that the effect of solvent thermodynamic power plays a minor role in the local chain dynamics of PNMA, since the activation energy for conformational transitions, E^*, and the rate of local dynamics scaled by viscosities (Figure 9b) are the same for the three solvents regardless of their thermodynamic power.

Solvent Effects on the Photophysical Behavior. Solvent effects on the photophysical behavior of poly(1-naphthylalkyl methacrylate)s and poly(1-naphthylalkyl acrylate)s have not been investigated systematically, and very few experimental data exist in the literature. However, in light of the present analysis some general remarks can be made in relation to the influence of the solvent on the photophysical properties of poly(1-naphthylalkyl acrylate)s.

Solvent effects on excimer formation and intramolecular energy migration in polymer systems containing naphthyl chromophores have been interpreted on the basis of the thermodynamic character of the solvent.[5,38] The excimer intensity and the rate of excimer formation increase with decreasing thermodynamic character of the solvent. This is attributed to the fact that the polymer chain contraction induced by poor solvents results in a greater number of naphthalene chromophores per unit volume and hence in an easier path to the formation of excimer pairs. This is

what has been observed[5,38] for poly(1-naphthyl methacrylate) in solution. However, for poly(1-naphthyl acrylate) (PNA), the excimer intensity and the rate of excimer formation are virtually independent of solvent.[5] For this polymer, the rate of excimer formation, k_{DM}, is 1.2×10^9 s^{-1} in EtOAc and 1×10^9 s^{-1} in CH_2Cl_2 at 23 °C. This difference in the rate of excimer formation between these two polymers has been attributed[5] to the increased flexibility of the acrylate main chain as compared to the methacrylate chain upon the removal of the α-methyl group.

Although the removal of the α-methyl group makes nearest neighbor naphthyl group approach far less hindered, the rate of the backbone local motions in PNA has been found[4] to be much slower (about 2 orders of magnitude) than the rate of excimer formation, and hence this motion does not influence significantly excimer formation. It is the side-chain motion, and in particular the naphthyl internal rotation characterized by comparable rate to that of excimer formation, that plays an important role in bringing two chromophores in the sandwich-like position that favors the formation of excimers.[4]

The present analysis shows that naphthyl internal motion is strongly dependent on solvent viscosity. Therefore, it is expected that in solvents of similar viscosities, such as EtOAc (η = 0.455 cP at 20 °C) and CH_2Cl_2 (η = 0.433 cP at 20 °C), excimer formation should be characterized by nearly equal rates, as has been observed experimentally for PNA.

Acknowledgment. We gratefully acknowledge financial support from the British Council and NATO (Grant No. CRG 910406). SERC (U.K.) provided funding for the 500 MHz instrument.

References and Notes

(1) Guillet, J. E. *Polymer Photosynthesis and Photochemistry*; Cambridge University Press: Cambridge, U.K., 1985.
(2) Semerak, S. N.; Frank, C. W. *Adv. Polym. Sci.* **1983**, *54*, 33.
(3) Spyros, A.; Dais, P.; Heatley, F. *Makromol. Chem.*, in press.
(4) Spyros, A.; Dais, P.; Heatley, F. *Macromolecules*, in press.
(5) Aspler, J. S.; Guillet, J. E. *Macromolecules* **1979**, *12*, 1082.
(6) Kramers, H. A. *Physica* **1940**, *7*, 284.
(7) Glowinkowski, S.; Gisser, D. J.; Ediger, M. D. *Macromolecules* **1990**, *23*, 3520.
(8) Lang, M. C.; Laupretre, F.; Noel, C.; Monnerie, L. *J. Chem. Soc., Faraday Trans.* 2 **1979**, *75*, 349.
(9) Waldow, D. A.; Ediger, M. D.; Yamagushi, Y.; Matsushita, Y.; Noda, I. *Macromolecules* **1991**, *24*, 3147.
(10) Meiboom, S.; Gill, D. *Rev. Sci. Instrum.* **1958**, *29*, 688.
(11) Ernst, R. R. *J. Chem. Phys.* **1966**, *45*, 3845.
(12) Craik, D. J.; Kumar, A.; Levy, G. C. *J. Chem. Int. Comput. Sci.* **1983**, *1*, 30.
(13) Dais, P. *Carbohydr. Res.* **1987**, *160*, 73.
(14) Radiotis, T.; Brown, G. R.; Dais, P. *Macromolecules* **1993**, *26*, 1445.
(15) Spyros, A.; Dais, P. *Macromolecules* **1992**, *25*, 1062.
(16) Gutnell, J. D.; Glasel, J. A. *J. Am. Chem. Soc.* **1977**, *99*, 42.
(17) Lyerla, J. R.; Levy, G. C. *Top. Carbon-13 NMR Spectrosc.* **1974**, *1*, 79.
(18) Sherwood, M. H.; Facelli, J. C.; Alderman, D. W.; Grant, D. M. *J. Am. Chem. Soc.* **1991**, *113*, 750.
(19) Heatley, F. *Prog. NMR Spectrosc.* **1979**, *13*, 47.
(20) Riseman, J.; Kirkwood, J. G. *J. Chem. Phys.* **1949**, *16*, 442.
(21) Dejean de la Batie, R.; Laupretre, F.; Monnerie, L. *Macromolecules* **1988**, *21*, 2045.
(22) Hall, C. K.; Helfand, E. *J. Chem. Phys.* **1982**, *77*, 3275. Weber, T. A.; Helfand, E. *J. Phys. Chem.* **1983**, *87*, 2881.
(23) Howarth, O. W. *J. Chem. Soc., Faraday Trans. 2* **1979**, *75*, 853.
(24) Spyros, A.; Dais, P. *J. Polym. Sci., Polym. Phys. Ed.*, submitted.
(25) Wittebort, R. J.; Szabo, A. *J. Chem. Phys.* **1978**, *69*, 1722.
(26) Gisser, D. J.; Glowinkowski, S.; Ediger, M. D. *Macromolecules* **1991**, *24*, 4270.
(27) Velsko, S. P.; Waldeck, D. H.; Fleming, G. R. *J. Chem. Phys.* **1983**, *78*, 249. Velsko, S. P.; Fleming, G. R. *J. Chem. Phys.* **1982**, *76*, 3553. Courtney, S. H.; Fleming, G. R. *J. Chem. Phys.* **1985**, *83*, 215.
(28) Bagchi, B.; Oxtoby, D. W. *J. Chem. Phys.* **1983**, *78*, 2735.
(29) Helfand, E. *J. Chem. Phys.* **1971**, *54*, 4651.
(30) Grote, R. F.; Hynes, J. T. *J. Chem. Phys.* **1980**, *73*, 2715.
(31) Guillermo, A.; Dupeyre, R.; Cohen-Addad, J. P. *Macromolecules* **1991**, *24*, 4270.
(32) Courtney, S. H.; Fleming, G. R. *Chem. Phys. Lett.* **1984**, *103*, 443.
(33) Cowie, J. M. G.; Ferguson, R. *Polymer* **1987**, *28*, 503.
(34) Heijboer, J.; Baas, J. M. A.; van de Graaf, B.; Hoefnagel, M. A. *Polymer* **1987**, *28*, 509.
(35) Montgomery, J. A., Jr.; Chandler, D.; Berne, B. J. *J. Chem. Phys.* **1979**, *70*, 4056.
(36) Waldow, D. A.; Johnson, B. S.; Hyde, P. D.; Ediger, M. D.; Kitano, I.; Ito, K. *Macromolecules* **1989**, *22*, 1345.
(37) Waldow, D. A.; Ediger, M. D.; Yamaguchi, Y.; Matshushita, Y.; Noda, I. *Macromolecules* **1991**, *24*, 3147.
(38) Abuin, E. A.; Lissi, E. A.; Gargallo, L.; Radic, D. *Eur. Polym. J.* **1979**, *15*, 373.